Thermo-mechanical response of near-pearlitic steel heated under restriction of thermal expansion

Journal of Materials Research and Technology 32 (2024) 1714–1724

Contents lists available at ScienceDirect

Journal of Materials Research and Technology

journal homepage: www.elsevier.com/locate/jmrt

Thermo-mechanical response of near-pearlitic steel heated under restriction of thermal expansion

Erika Steyn, Johan Ahlström *

Department of Industrial and Materials Science, Chalmers University of Technology, 412 96, Gothenburg, Sweden

ARTICLE INFO

Keywords:
Railway wheel steel (ER7T)
Near-pearlitic microstructure
Thermo-mechanical fatigue TMF
Spheroidization
Severe block braking
Residual stress

ABSTRACT

Railway wheels experience high temperatures during operation, especially during severe block braking. The thermal expansion of wheel rim material due to frictional heating is limited by the wheel's geometry and size. This study investigated the impact of this combined mechanical and thermal loading on the mechanical properties and microstructure in the tread surface of an ER7T steel railway wheel.

The material response below the austenitisation temperature is comprehensively evaluated through thermal cycling at peak temperatures of 300, 400, 600, and 650 °C, simulating severe block braking cycles with varying degrees of thermal dilatation (25 %, 50 %, 75 %, and 100 %). An initial plastic deformation was observed during the first heating cycle for the two lower temperatures at lower restrictions, followed by a predominantly elastic response. However, at higher restrictions, the material showed time-dependent relaxation during heating, and some plastic deformation was observed during cooling. Notably, even at the lowest level of restriction, similar observations were made at higher peak temperatures. Increasing the restriction resulted in large strains and a wider hysteresis loop. The test bars exposed to the two higher temperatures retained large tensile stresses after cooling. This indicates a risk of a significantly altered residual stress state in the rim of an overheated railway wheel, which could adversely affect its fatigue properties. The study's outcomes will aid in designing and calibrating constitutive material models for severe block braking. Furthermore, it will significantly contribute to research into the thermo-mechanical behaviour of pearlitic/near-pearlitic materials during railway operations and maintenance.

1. Introduction

Pearlitic and near-pearlitic steels are used in a wide range of applications, including railway wheels and rails. In Europe, ER7T is a commonly used material grade in the production of railway wheels for freight trains. This near-pearlitic medium carbon steel is tailored to provide good strength and wear resistance in the wheel-rail interface [1,2]. The integrity of the railway system depends on the quality of this wheel-rail interface; therefore, it is important to understand the degradation mechanisms of both the wheel and rail material.

High temperatures can develop during operation, especially in the wheel rim during tread braking. This can have detrimental effects on the microstructure and mechanical behaviour of the wheel steel. The near-pearlitic microstructure is susceptible to spheroidisation of the cementite lamella in pearlite at elevated temperatures [3], resulting in decreased hardness and strength. Additionally, the restriction of thermal expansion during the braking operation induces mechanical strain, which essentially generates an applied compressive hoop stress at elevated temperatures. The combination of plastic deformation and elevated temperatures can lead to an even higher tendency for spheroidisation [4–6].

The material degradation under isothermal low cycle fatigue conditions [7–9], rolling-sliding contact loading [10] and the thermo-mechanical fatigue damage on railway brake discs [11] have previously been investigated. The effects of thermo-mechanical processing on the microstructure and properties of steels and irons have also been studied for other applications [12–14] – this is of particular interest for tool steels [15,16]. However, there is a need for additional experimental research into the behaviour of railway materials during operations such as severe block braking on railway wheel steel. This need is emphasised by studies showing that the residual stress state within the wheel tread is difficult to predict [17–20].

This study will focus on the cyclic behaviour and material degradation of the railway wheel steel ER7T during thermo-mechanical loading

* Corresponding author.
E-mail addresses: erika.steyn@chalmers.se (E. Steyn), johan.ahlstrom@chalmers.se (J. Ahlström).

https://doi.org/10.1016/j.jmrt.2024.07.107
Received 8 April 2024; Received in revised form 20 June 2024; Accepted 17 July 2024
Available online 31 July 2024

imitating block braking. The effect of thermal dilatation restriction to different degrees during thermal cycling is investigated. The measured mechanical response was used to calibrate a model for severe block braking in a parallel work [21].

2. Material and methods

Railway wheel material ER7T with chemical composition as per EN 13262 [22] was used for this study (see Table 1). Rim chilling during production allows for a fine-pearlitic microstructure close to the wheel tread and ensures a harder and stronger material in the wheel rim than in the web and hub sections of the wheel, along with a compressive residual stress state in the near surface layer. At 20 mm depth below the surface of a new wheel, the lamellar spacing is around 125 nm, and the free (pro-eutectoid) ferrite content is about 10 %. The ferrite content as well as the pearlite lamellar spacing increase slowly with an increase in depth, resulting in a slight gradual reduction of hardness [7].

This study evaluates the effect of thermo-mechanical cycling on unused ER7T wheel material with samples taken from the rim, some 15 mm below the central part of the running surface (the so-called tread datum). The rim material is exposed to different temperatures due to the severity and longevity of block braking and samples were therefore tested at peak temperatures up to 650 °C. Cylindrical test bars with a gauge diameter of 10 mm were machined according to the dimensions as shown in Fig. 1.

2.1. Thermo-mechanical cycling

Uniaxial thermo-mechanical testing according to the Thermo-Mechanical Fatigue (TMF) Code-of-Practice for strain-controlled testing [23] was performed using an MTS 809 servo-hydraulic biaxial test frame; rotation was restricted during this test series. The sample setup is shown in Fig. 2(a). Induction heating is used, with the red induction coil as seen in the figure, and the temperature was measured using two K-type thermocouples welded onto the test bar - the control thermocouple is exactly in the centre of gauge length and the monitoring thermocouple on the test bar radius is used for the safety interlock. Strain was measured with an MTS water-cooled high-temperature extensometer with ceramic extension rods. The approach followed for this thermo-mechanical testing is summarised in the flow diagram Fig. 2 (b) and described below.

A numerical model of tread braking temperatures was developed in Refs. [24–26] using measurements from field studies on the severe block braking of freight wheels. This was presented as a temperature cycle with a maximum of 650 °C reached after 45 min heating, followed by about 60 min of cooling. In this study, a parametrised temperature curve, with two exponential functions describing the heating and cooling rates respectively, was developed. Typically, the rim material would seldomly be exposed to peak temperatures close to 600 °C; in normal operation, braking cycles will result in much lower peak temperatures. Therefore, different peak temperatures (T_1) were evaluated by using a scaling factor, k, set relative to the peak temperature of 650 °C, to mimic different braking cases. In other words, $k = T_1/650$. The duration of the temperature cycles was kept the same for all peak temperatures. The parametrised expressions are shown below:

$$\begin{aligned} T_H &= -700ke^{-0,00098x} + 700k \\ T_C &= 3300ke^{-0,00056x} - 40k \end{aligned} \quad (1)$$

with T_H indicating the temperatures on the heating curve, T_C the temperatures for the cooling curve and x the time (in seconds). Temperature control below 50 °C proved difficult with induction heating due to large ambient temperature variations; therefore, after the first test of rim material with a base level of 30 °C, 50 °C was set as baseline temperature. The simulated worst-case scenario indicated that the induced mechanical strain during block braking can vary between 30 % and 60 % of the thermal strain, depending on the location in the wheel [21]. Therefore, the tests were set up to restrict the thermal dilation to varying degrees, ranging from full restriction (mechanical strain set to 100 % of thermal strain) to free expansion (mechanical strain is set to zero).

For each test series, thermal compensation factors for compliance with the TMF Code-of-Practice were determined from a zero-stress test using repeated heating cycles. Using a Matlab script, thermal compensation factors were determined by regression analysis. The compensation factors are entered in the test control software, which uses it for calculating the thermal strain ($\varepsilon_{thermal}$) based on the temperature feedback (T) measure by the control thermocouple (following Equation (2)); the polynomial coefficients E_2, E_1 and E_0 used are shown in Table 2.

$$\varepsilon_{th} = \boldsymbol{E_2}T^2 + \boldsymbol{E_1}T + \boldsymbol{E_0} \quad (2)$$

Quantified thermal dilatation under zero-stress conditions are necessary for well-defined restriction of thermal dilatation during testing. Fig. 3 illustrates the test procedure. The zero-stress test (ZST) is an initial test performed for each test series where full expansion is allowed. The controller is used to maintain zero axial force and the total measured strain is therefore equal to the thermal strain ($\varepsilon_{thermal}$). Thermal compensation is then tuned to remove this thermal expansion, so that the total strain in subsequent tests would equal an applied mechanical strain (ε_{mech}). After a correct introduction of thermal compensation factors, a strain-controlled test with zero mechanical strain, gives very low force in the test bar. This verifying test is called the zero-stress test evaluation (ZSTE) run and the max allowed stress is prescribed in the TMF Code-of-Practice. In this study, the effect of restriction of thermal dilatation was investigated. This was done by applying mechanical strain to counter-act the thermal compensation, as indicated by the red (leftward) arrows in Fig. 3. Case **a** in the figure represents the zero-stress test evaluation (ZSTE) where free expansion is simulated by applying mechanical strain equal to 100 % of the thermal strain as measured during the initial ZST; i.e. the restriction for case **a** is 0. Cases **b** to **e** show tests with different degrees of the thermal dilatation restriction, from 25 % for case **b** up to 100 % for the zero total strain (ZTS) test for case **e.**

After calibration, strain-controlled tests of five cycles each were performed at varying levels of mechanical strain, calculated as 0, 25, 50, 75 and 100% of the thermal strain, based on the employed thermal compensation. In essence, this corresponds to restricting thermal dilatation to different degrees. Four test series were completed at peak temperatures of 300, 400, 600 and 650 °C.

2.2. Hardness testing and microstructural evaluations

Samples were taken from the gauge section of each test bar as well as from the end of the grip section of each test bar to represent the thermo-mechanically exposed material as well as the virgin material (not strained nor heated). Metallographic preparation was done by mechanical polishing down to 1 μm with a diamond solution and a final active oxide (colloidal silica) polishing step to 0.04 μm. Room temperature hardness measurements were performed using a Vickers hardness (HV) load of 30 kg on a Struers/Emcotest DuraScan-70 G5 hardness

Table 1
Chemical composition of railway wheel material ER7/ER7T [22].

	C	Si	Mn	Mo*	Cr*	Ni*	S	P	V	Cu	Fe	*Mo + Cr + Ni
[wt %, max]	0.52	0.4	0.8	0.08	0.3	0.3	0.015	0.02	0.06	0.3	Bal	0.5

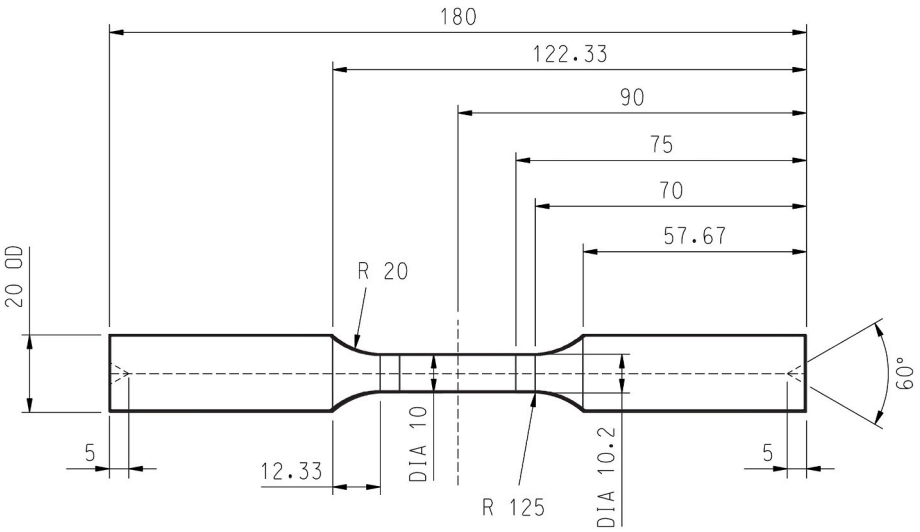

Fig. 1. Standard test bar geometry.

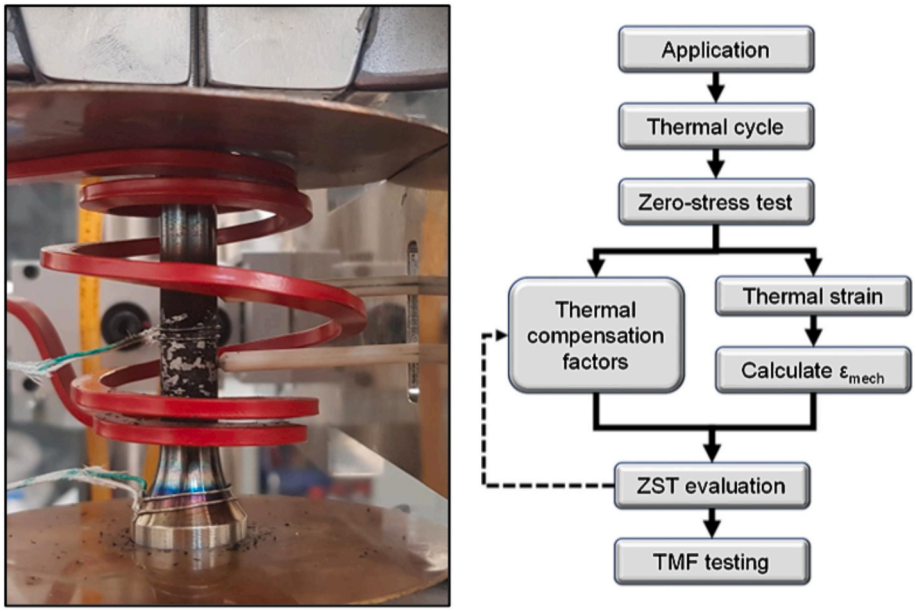

Fig. 2. a) Experimental setup (b) Thermo-mechanical fatigue testing procedure.

Table 2
Parameters used for thermal compensation (*10^6).

Temperature	E_2	E_1	E_0
300 °C	0.013	7.49	−43
400 °C	0.007	10.20	−245
600 °C	0.003	12.43	−374
650 °C	0.004	12.29	−350

tester. At least five indentations were made randomly on each sample surface and the hardness value was taken as the mean of the measured values. Polished samples were etched using a 3 % Nital solution (HNO_3 in ethanol) and investigated using a LEO Gemini 450 field emission gun scanning electron microscope (FEGSEM).

3. Results and discussion

3.1. Cyclic thermo-mechanical behaviour

First, we display and discuss the stress development during the tests, and then go more into detail examining the stress vs temperature loops to sort out certain details on elastic vs plastic or viscoplastic deformations.

Fig. 4 shows the stress development for the rim material exposed to a thermal cycle with a peak temperature of 300 °C and a base level of 30 °C. The zero-stress evaluation run (blue curve) is included as a confirmation that the thermal compensation procedure adopted works sufficiently well for the tests to conform to the TMF Code-of-Practice [23]. A small initial tensile stress peak to 60 MPa is seen when the first heating cycle starts, but thereafter stress is maintained at low mean stress (≈8 MPa) and with a small amplitude (<20 MPa). The result for the fully restricted test (green curve) shows first an elastic response with increasing temperature, i.e., stresses are arising proportionally to the

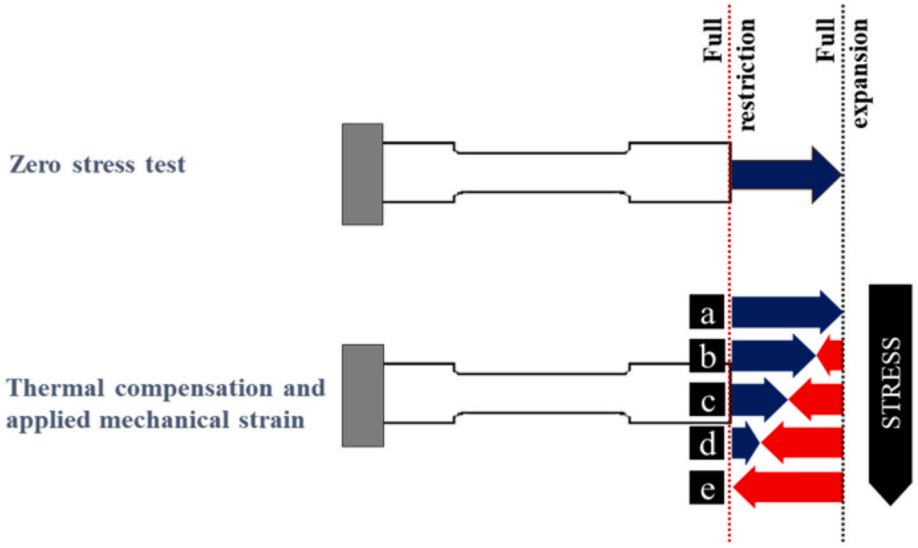

Fig. 3. Illustration of thermal compensation and strain application during thermo-mechanical testing.

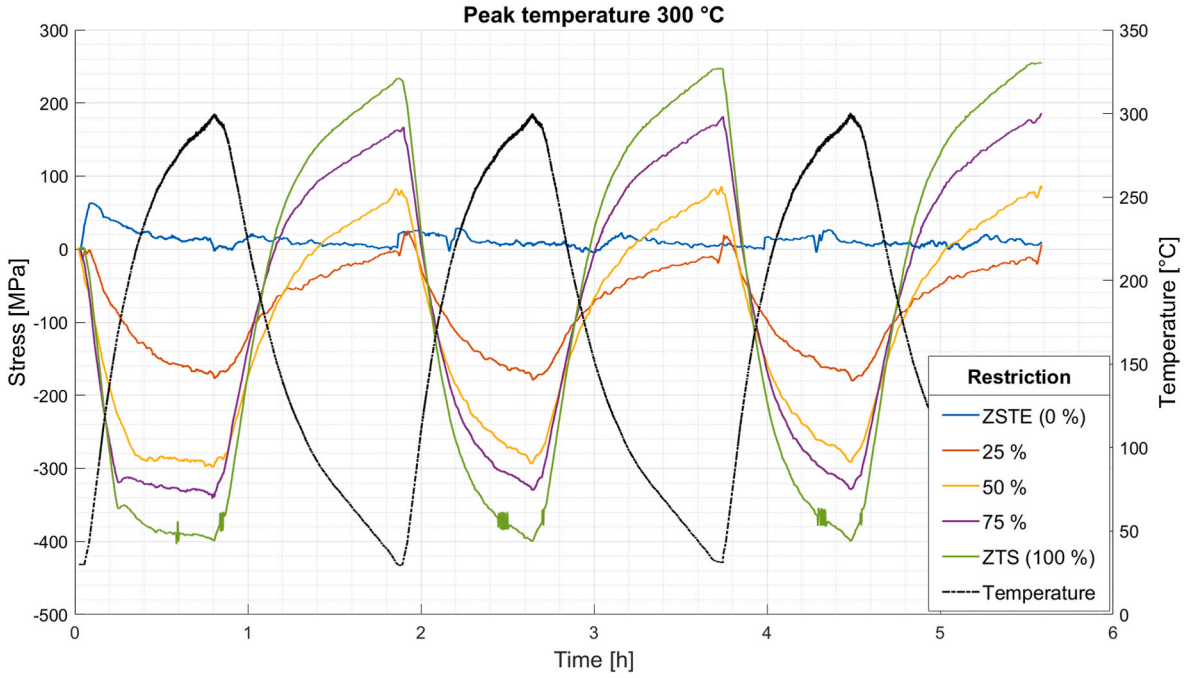

Fig. 4. Influence of thermal dilatation restriction on stress during thermal cycling for a peak temperature of 300 °C.

thermal expansion. At around 150 °C, plastic deformation starts when thermal dilatation causes a strain large enough to plasticise the material at that temperature and strain rate, around −350 MPa (not directly comparable to yield stress, since stress relaxation occur in this type of material at low strain rates [7]). After first yielding a gradual increase in compressive stress follows and reaches a maximum absolute value at −400 MPa. Upon cooling, thermal contraction causes a proportionally increasing stress with respect to the temperature decrease. The second cycle starts in a similar way, but plastic deformation in compression is not seen; instead, the relation between heating and stress build-up due to thermal expansion is proportional. This signifies a strong hardening effect in the first cycle which is most probably due to static and dynamic strain ageing phenomena (cf [7,27]). On cooling and further cycling, the pattern repeats and cycles are alike except for a small gradual increase in peak tensile stress, probably explained by accumulating strain ageing effects. It is reasonable that the peak stress in tension is much lower than the absolute value of the trough stress in compression, considering the plastic deformation in the first cycle; this could be modelled as a kinematic hardening contribution translating the centre of the yield surface to ca −80 MPa.

The 75 % restricted test shows a very similar behaviour with modified stress levels. Decreasing restriction to 50 % leads to less marked initial yielding, but otherwise analogous behaviour. At 25 % restriction, no plastic deformation is observed. The anomalies seen in the flow curve of the fully restricted test every time temperature passes ca 270 °C could possibly be related to dynamic strain ageing induced serrated yielding (the "Portevin-Le Chatelier effect"). The peak compressive stresses are remarkably stable for all restriction levels while a slight increase in peak stress is observed; i.e. strain ageing effects seem to build-up but cannot overcome the stress relaxation at the highest temperature.

Fig. 5 shows the stress development vs time for the rim material exposed to a thermal cycle with a peak temperature of 400 °C and a base level of 50 °C. The zero-stress evaluation run (blue curve) shows an initial tensile stress peak of 80 MPa when the heating cycles start; thereafter, stress is maintained at low mean stress (≈0 MPa) with a small amplitude (<10 MPa). The result for the fully restricted test (green curve) also here shows an initial elastic response with increasing temperature. Yielding is gradual, without yield phenomena, with plastic deformation starting around 200 °C at a compressive stress level of ca −420 MPa. The higher strain rate due to higher heating rate relative to the test with peak temperature 300 °C, gives less time for stress relaxation which could explain the higher stress level. The compressive stress reaches a maximum value of about −460 MPa at 320 °C, and thereafter stress relaxation proceeds faster than the slowly increasing thermal strain resulting in a decreasing stress level. Thermal contraction during cooling causes an increase in stress proportional to the temperature decrease, just as in the case of 300 °C peak temperature. Due to a short delay at the low temperature, a hold period is induced. Little plastic or viscoplastic deformation is observed in the second cycle, reaching the maximum compressive stress of −420 MPa at the peak temperature (400 °C). Subsequent cycles follow a similar pattern except for a small increase in peak tensile stress for each cycle. An apparent symmetry in peak/trough stress can be observed with approximately 0 MPa mean stress and a 400 MPa amplitude.

The 75 % restriction test shows a similar behaviour but with scaled stress levels and a small negative mean stress. At 25 % restriction, no significant yielding or plastic deformation is observed, and stresses generated are proportional to the thermal dilatation. The 50 % restriction test is somewhere in between the 75 % and 25 % test; since the driving force for stress relaxation in the hot part of the cycle is smaller than in the 75 % and 100 % tests, a significant negative mean stress of over 100 MPa develops. The anomalies seen in the 50 % restriction and 25 % restriction tests every time a new cycle starts are most likely caused by the sudden change in test bar temperature distribution when induction heating is applied after the hold period and is similar to what can be seen in the zero-stress test response.

In Fig. 6 the stress development for a peak temperature of 600 °C and a base level of 50 °C is depicted. The zero-stress evaluation run (blue curve) varies systematically during the test with a stress amplitude of 40 MPa, which is still within the allowed margins of the Code-of-Practice [23]. The fully restricted test (green curve) shows gradual initial yielding, but after a peak compressive stress of about −460 MPa at 320 °C (same as for the 400 °C case) it shows stronger stress relaxation at increasing temperature leading to gradually lower stress response – at the highest temperature, stress is below −100 MPa. Thermal contraction during cooling causes an increase in stress proportional to the temperature decrease. Because of the significantly larger temperature range in combination with “shortening” of the test bar at high temperature, the peak tensile stresses are much larger than in tests at lower peak temperatures. The second cycle shows a decrease in the maximum compressive stress, with the peak at about −225 MPa and 475 °C, suggesting material softening during the first cycle (which is expected based on earlier studies on spheroidisation [6]) in combination with translation of the yield surface.

The 75 % restriction and 50 % restriction tests show similar behaviour with scaled stress levels; deviations in stress response approaching 50 °C in the 50 % curve were due to machine control issues. At 25 % restriction, the maximum compressive stress is about −220 MPa at 475 °C in the first cycle and some plastic deformation is observed. Subsequent cycles (from cycle 2 onwards) for all levels of restriction follow a similar stress-time relationship; judging from this stable behaviour, most microstructural changes seem to occur already during the first heating phase. Serrations are seen in each tensile stress cycle at about 450 MPa for both the full restriction (around 260 °C) and 75 % restriction (around 225 °C) tests – as for the 300 °C peak temperature case, this could possibly be related to dynamic strain ageing and serrated flow. Another anomaly is seen in the 75 % restriction test at the peak compressive stress of about −170 MPa (between 460 °C and 510 °C).

Fig. 7 shows the stress development for a thermal cycle with a peak temperature of 650 °C and a base level of 50 °C. In principle, the results are similar to the tests at 600 °C. The first heating cycle has an initial tensile stress peak of 120 MPa in the zero-stress evaluation run (blue curve). However, the low mean stress (≈−5 MPa) and stress amplitude of about 25 MPa in following cycles still falls within the acceptable margins of the Code-of-Practice [23]. The result for the fully restricted test (green curve) shows that plastic deformation starts at around 200 °C and −365 MPa, and that the peak compressive stress is reached at about −380 MPa at 350 °C. Thermal contraction during cooling causes an

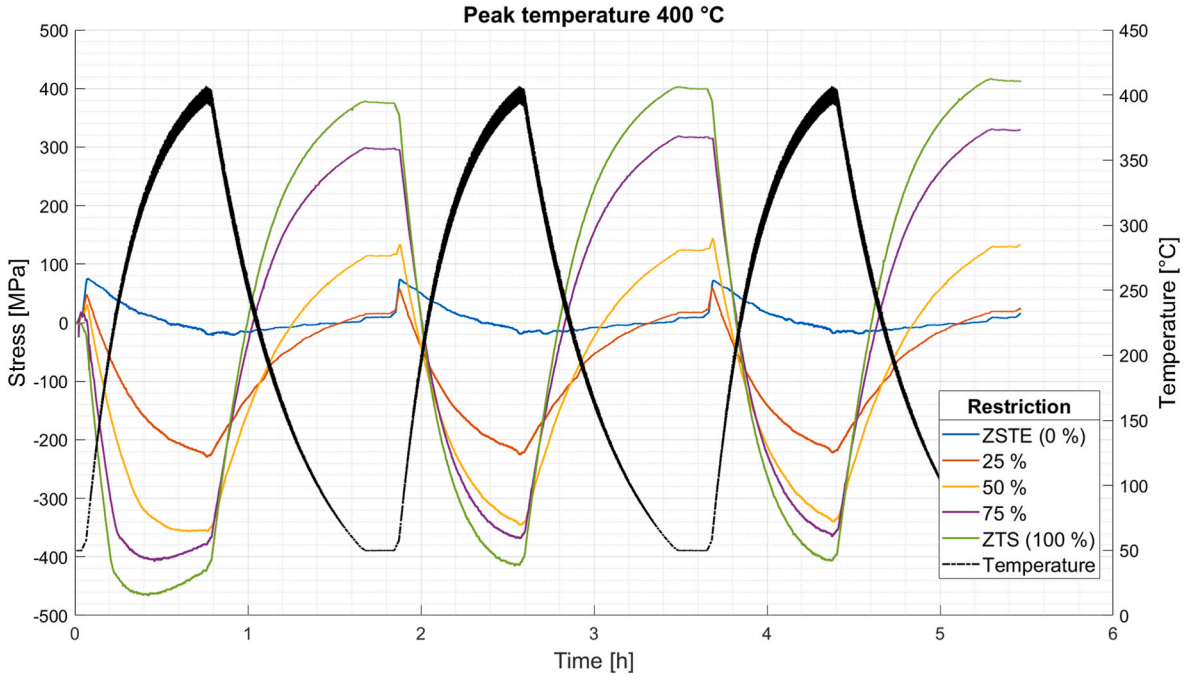

Fig. 5. Influence of thermal dilatation restriction on stress during thermal cycling for a peak temperature of 400 °C.

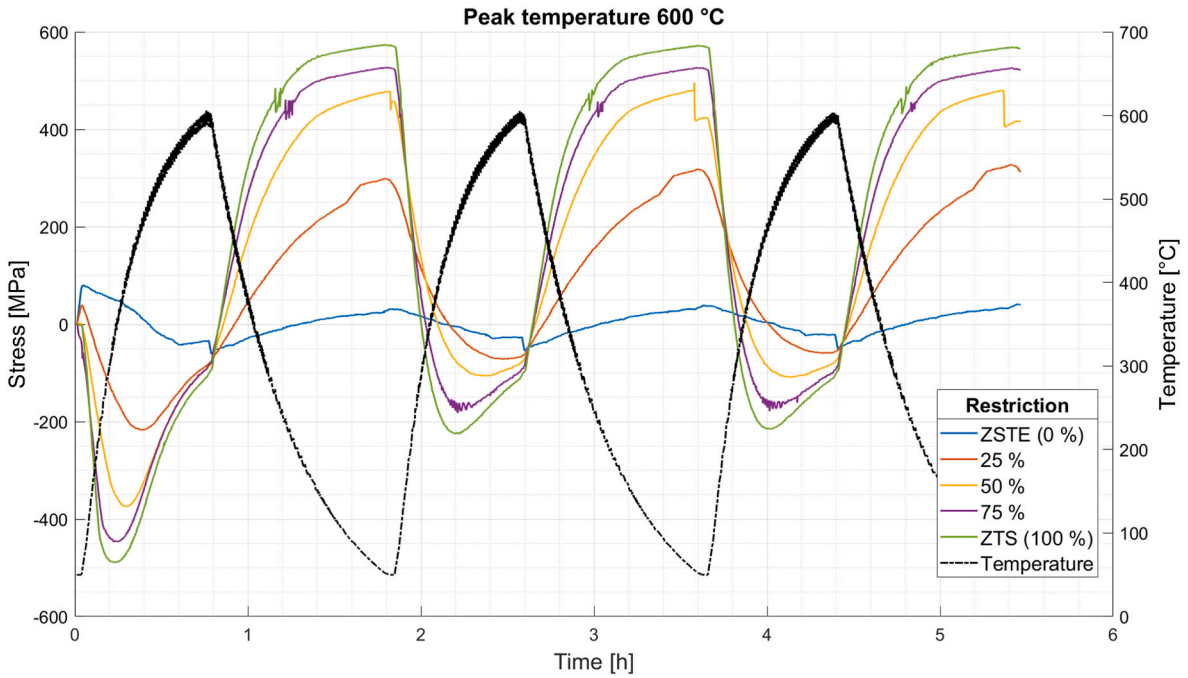

Fig. 6. Influence of thermal dilatation restriction on stress during thermal cycling for a peak temperature of 600 °C.

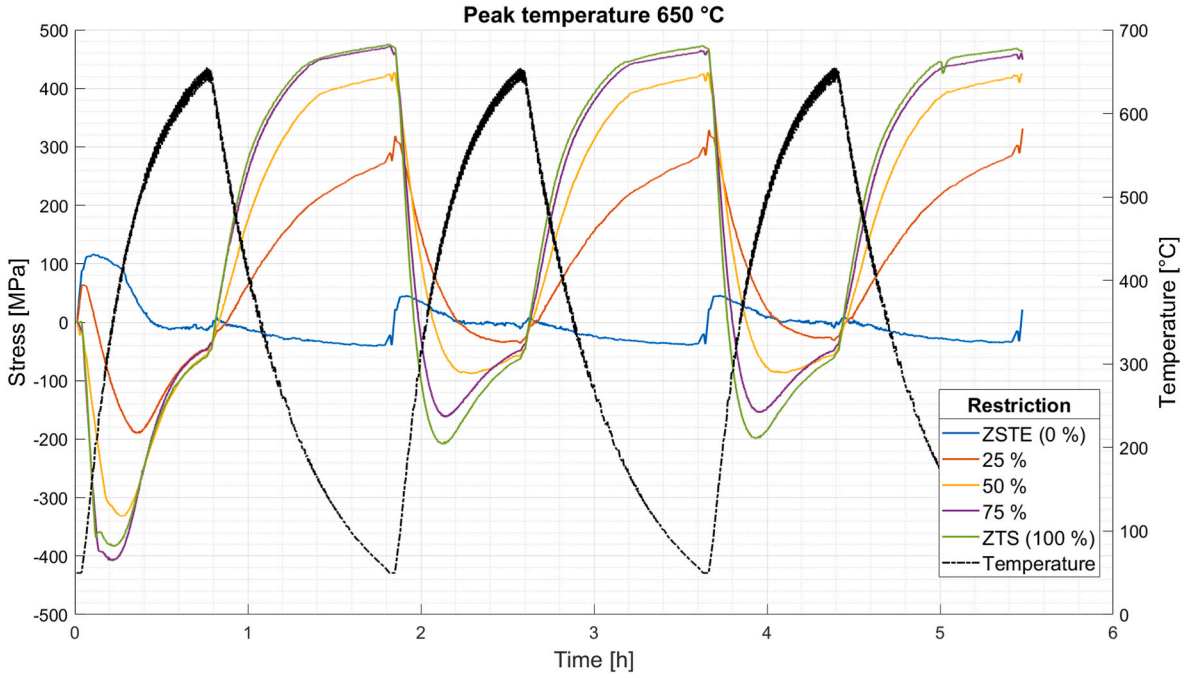

Fig. 7. Influence of thermal dilatation restriction on stress during thermal cycling for a peak temperature of 650 °C.

increase in stress proportional to the temperature decrease. The second cycle shows a decrease in the maximum compressive stress, with the peak at about −210 MPa and 430 °C, indicating permanent material softening after the first cycle (mainly due to spheroidisation). On cooling and further cycling, the pattern repeats. The 75 % restriction and 50 % restriction tests show similar behaviour with scaled stress levels. At 25 % restriction, an initial tensile peak of about 60 MPa is seen which correlates with the zero-stress evaluation run anomaly; thereafter the stress becomes compressive to a maximum of about −190 MPa at 480 °C in the first cycle.

Fig. 8 shows the stress response versus the temperature for the two lower peak temperatures. Straight lines are inserted to help sort out how elastic stress increase caused by thermal dilatation would appear. The slope is adapted to the degree of thermal strain vs total strain (restriction) and is based on an anticipated coefficient of linear thermal expansion of 14·10–6/°C and a Young's modulus of 200 GPa. The position is adapted to fit the first thermal loading. Here it can be seen that the first cycle of each test typically exhibits an initial elastic response as long as the imposed stress is low enough for the material not to plasticise, i.e. d(σ)/d(T) aligns with the expected thermal dilatation. In Fig. 8 (a)–(d) this response is observed for a peak temperature of 300 °C. Initial plastic deformation is seen as a saturation of stress towards higher

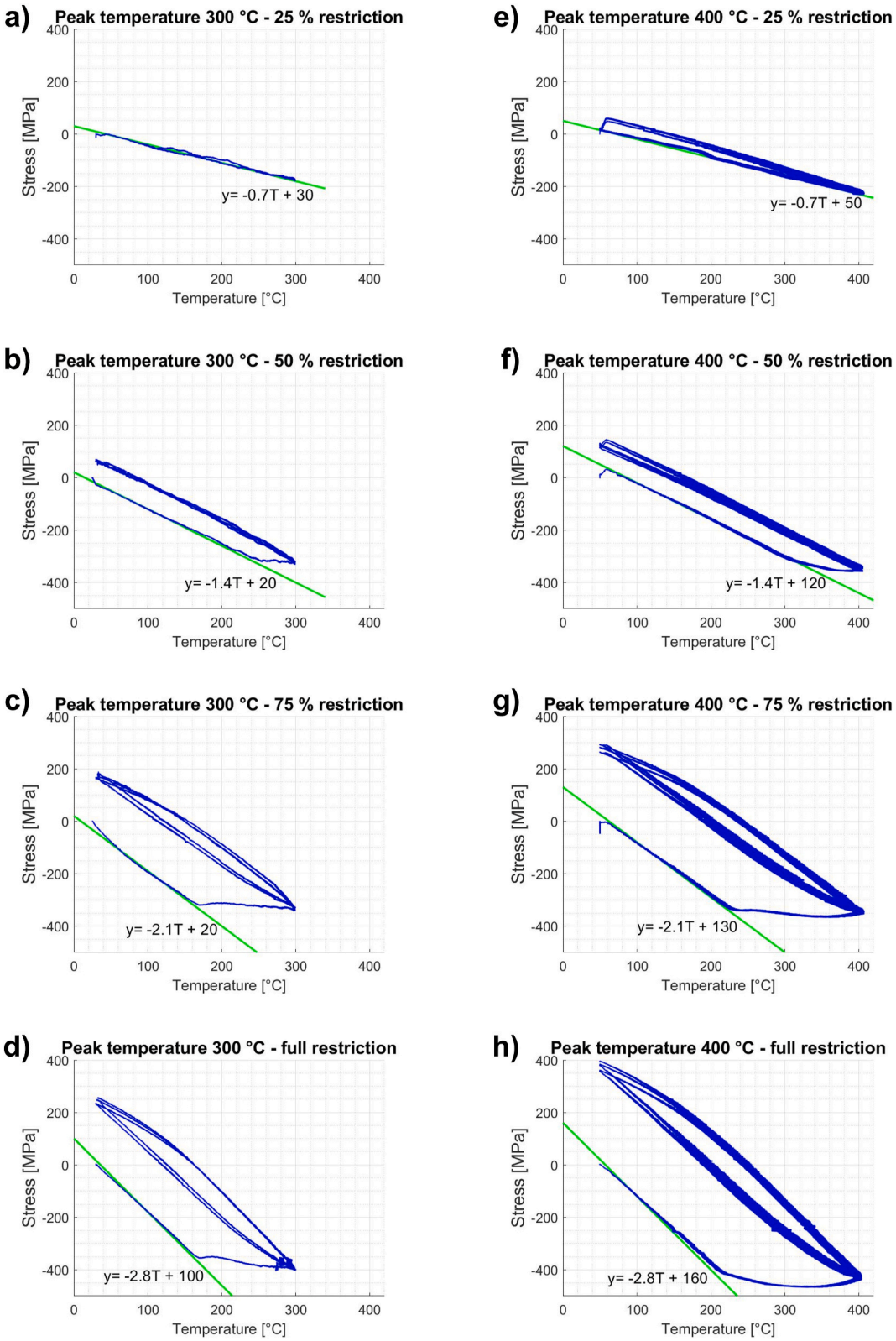

Fig. 8. Stress response with variation in peak temperatures and degree of thermal dilatation. (a) To (d) shows the stress response for a peak temperature of 300 °C and (e) to (h) shows the stress response for a peak temperature of 400 °C.

temperatures. At the two higher restriction levels, further temperature cycling leads to a small hysteresis loop, while the case with 50 % restriction deviates from non-linearity in the first cycle only. Fig. 8(e)–(h) shows the stress response for a peak temperature of 400 °C. The increase in temperature difference leads to a considerably higher tensile stress response at the lower temperature than in the case of peak temperature 300 °C. Comparing the amount of plastic deformation in terms of hysteresis loop width though, the difference is not large. This signifies hardening of the material, probably due to strain ageing being more efficient for the 400 °C peak temperature cycle.

In the cases with higher peak temperatures of 600 °C and 650 °C, as shown in Fig. 9(a)–(d) and (e) to (h) respectively, the behaviour becomes strongly influenced by pronounced relaxation of stresses, i.e., a viscoplastic response, cf for example [7,28]. The two curves corresponding to the lowest restriction levels, (a and e), show plastic flow and relaxation in the first cycle, thereafter the material is mostly elastically strained. In essence, this first heating ramp shortens the test bar, so that even if the microstructure is spheroidised and the material is soft at the highest temperatures, the following cycles do not generate significant compressive stress in the high temperature range 500–600 °C and thus

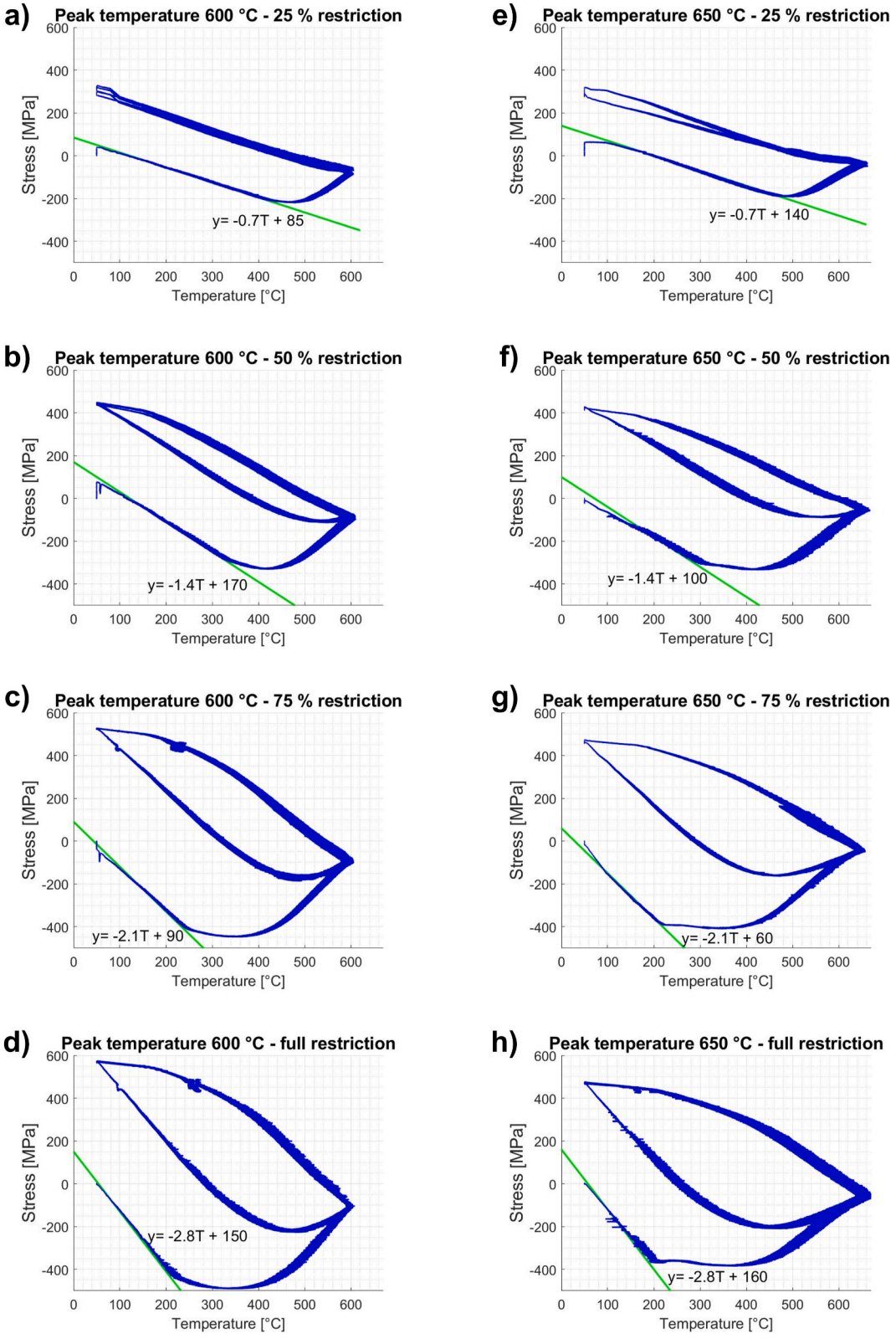

Fig. 9. Stress response with variation in peak temperatures and degree of thermal dilatation. (a) To (d) shows the stress response for a peak temperature of 600 °C and (e) to (h) shows the stress response for a peak temperature of 650 °C.

do not cause significant non-elastic strain. However, a slight stress relaxation seen as a deviation from the expected slope (green curve) is visible above 500 °C and there are some anomalies at the lowest temperatures, seen already in Figs. 6 and 7. Common for all restriction levels, the initial cycle causes plastic deformation and relaxation giving low compressive stresses at the peak temperature, ca −100 MPa for the tests with peak temperature 600 °C and ca −50 MPa at 650 °C. This is expected with such high temperatures and durations and is a typical behaviour of this type of material. As a comparison, consider isothermal cyclic straining tests with hold times at the peak compressive strain reported in Ref. [7].

A graph describing the actual relaxation with time for a test with conditions as described in that paper is depicted in Fig. 10. Another difference between the two test series, is the wider loops in the case for the higher peak temperature 650 °C. It could be noted the repeatability between the following cycles is very high, apart from some noise. The larger ranges of thermal strains imposed in the tests with peak temperatures of 600 and 650 °C, contribute to higher tensile stress levels reached on cooling than for the tests with lower peak temperatures (300 and 400 °C) for all levels of restriction. Another mechanism for this is the translation of the mean stress to positive levels in the range of 50–150 MPa. The peak compressive stresses in following cycles are low both due to spheroidisation decreasing the dispersion hardening mechanisms from cementite lamella and the stress relaxation at higher temperature. If this behaviour is related to railway engineering, it means that a severely overheated wheel could risk having large tensile stresses superimposed to the rolling contact loading in the rim material which has also a lower strength than before, increasing the risk for fatigue damage accumulation.

The situation is rather different for the moderately heated material. Especially the lower levels of restriction generate very low residual tensile stress after cooling down. Due to time spent in the temperature interval where strain ageing occurs, the material hardens slightly. Further experiments and modelling of operational conditions are required for firm conclusions and quantification of stresses after specific scenarios. Fig. 11 shows a summary of the stress results from the respective test series in the third thermal cycle. The solid lines show the stress range (i.e. difference between the peak stresses in tension and compression), while the dashed lines show the maximum tensile stress which remains in the material after cooling to room temperature.

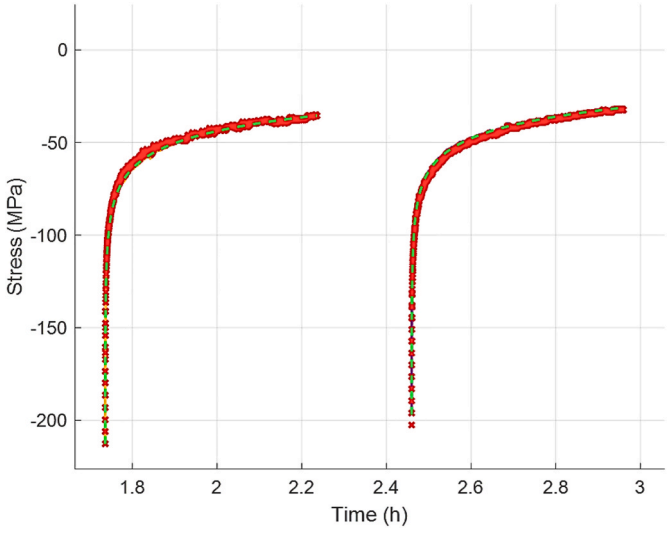

Fig. 10. Stress relaxation at 600 °C on static hold at −1.0 % strain during two 30 min periods. Before the hold periods, the material was exposed to strain-controlled cyclic loading with an amplitude $\Delta\varepsilon_t/2 = 1.0$ %). The graph has not been published before but the results are from a previous study; for experimental details, please refer to Ref. [7].

This shows that an increase of the restriction has a larger impact on the tests at lower temperatures. However, despite the smaller stress ranges seen for the high temperature tests, these test series result in consistently higher residual stresses after cooling to room temperature. This figure also shows the gradual increase in both stress range and residual stress with an increase in the degree of thermal dilatation restriction. Therefore, it is worthwhile designing wheels with as little restriction towards thermal strains as possible to avoid tensile residual stresses in the rim.

3.2. Microstructure and hardness

Micrographs of material extracted from the gauge sections of two test bars are shown as examples (compared to the virgin state) in Fig. 12. After testing at 300 °C without restriction, little or no spheroidisation is visible, with a median room temperature hardness of 252 HV (compared to approximately 260 HV for the virgin material). The normalised hardness values for the two lower temperatures are within ±6 % of the virgin hardness and typically higher after tests with more restriction due to more efficient strain ageing. I.e. there is little change from the virgin condition. This is expected since it corresponds to a normal heat treatment.

At 650 °C the degree of spheroidisation is strong, although not all areas are spheroidised. These observations are in accordance with previous studies on the same material of isothermal heat treatment after or during cyclic straining [5–7]. A notable reduction of 10 % ± 4 % (with hardness of about 240 HV) is observed in room temperature hardness after the higher temperatures 600 and 650 °C – this is expected, considering the high degree of spheroidisation. This is in line with previous tests on isothermally heat treated railway wheel steel [7]. A smaller variation in hardness is seen for different degrees of thermal dilatation restriction at higher temperatures.

The microstructural changes and time-dependent straining at the higher temperatures signifies that railway wheel steels are not suitable for high temperature applications. The relatively high remaining strength and hardness after cooling on the other hand, tells the microstructure is still capable of bearing significant monotonic loads also after overheating to temperatures above 600 °C; tensile stresses reaching over 500 MPa are reached after cooling in the thermo-mechanical experiments, and hardness loss at room temperature is limited to some 15 % which means strength is not too far from the un-used condition [29].

4. Conclusions

The influence of combined mechanical and thermal loading on the mechanical performance and microstructure of railway wheel steel ER7T was investigated at different peak temperatures corresponding to moderate overheating (300 and 400 °C) and severe overheating (600 and 650 °C) and at different levels of restriction of the thermal expansion (25 %, 50 %, 75 % and 100 %). The following conclusions can be drawn:

1. The microstructure and mechanical properties are not much changed after thermo-mechanical cycling to 300 and 400 °C peak temperature. But when the material is viscoplastically deformed in compression during the heating cycle, there is a remaining tensile stress in the test bar after cooling. This happens already at 50 % restriction and increases strongly with increasing restriction.
2. After thermo-mechanical cycling to 600 and 650 °C, the material is spheroidised, and loses some 10 % of its original room temperature hardness. At the peak temperature, stresses are relaxed to levels below 100 MPa in all cases. During following cooling, large tensile stresses are generated and remain in the test bars after cooling at all restriction levels.

Numerical predictions inspired the choice of restriction levels, and

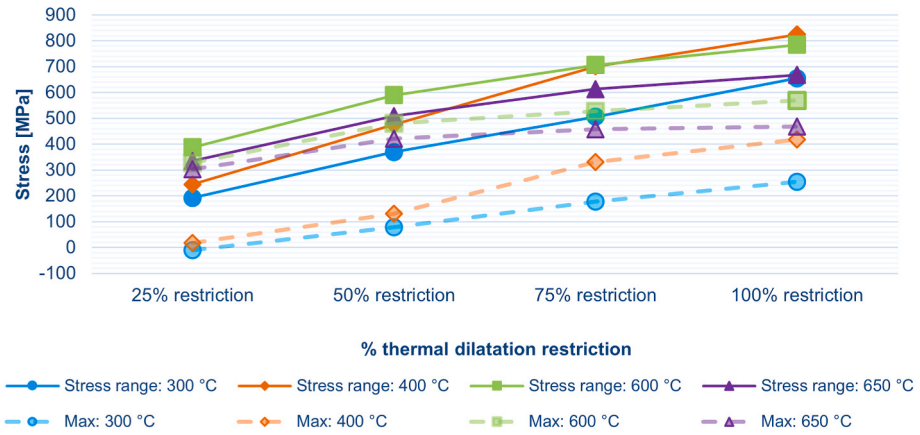

Fig. 11. A summary of the stress results from the respective test series in the third thermal cycle. The stress range for each test is represented by the solid lines, whereas the maximum residual stress expected at room temperature is shown with the dashed lines.

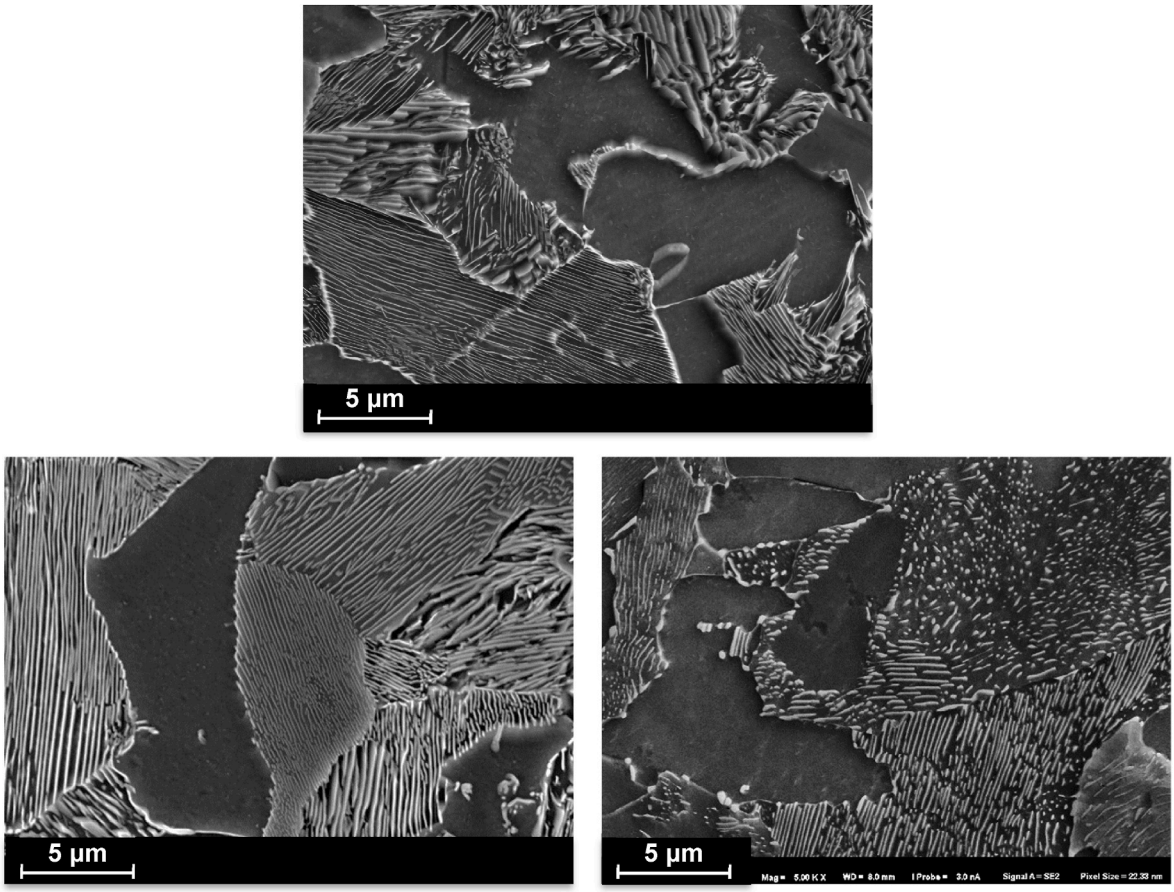

Fig. 12. SEM images of a virgin sample (top), a sample tested with free expansion at a peak temperature of 300 °C (bottom left) and a sample tested with full restriction at a peak temperature of 650 °C (bottom right).

up to 60 % restriction is mentioned as a reasonable maximum level in the application. For the cases examined, severe overheating would create large tensile residual stresses in the hoop direction of the wheel, and thus impact both wheel geometry (mainly the gauge width) and fatigue properties. Moderate overheating with restriction levels around 50 % does not seem to have very severe consequences on strength and hardness, and the material microstructure is retained. However, a consideration during the wheel design should be that compressive hoop stresses generated during production can be lost also during such moderate heating cycles.

Data availability statement

The raw/processed data required to reproduce these findings cannot be shared at this time as the data also forms part of an ongoing study.

Declaration of competing interest

The authors declare that they have no known competing financial interests or personal relationships that could have appeared to influence the work reported in this paper.

Acknowledgments

This research forms part of the activities within the Chalmers Railway Mechanics Centre of Excellence, CHARMEC (www.charmec.chalmers.se). Parts of the study have been funded from the European Union's Horizon 2020 research and innovation programme in the project In2Track3 under grant agreement 101012456 and in the Horizon Europe, Europe Rail project IAM4RAIL under grant agreement No. 101101966. The authors would like to thank Andrea Ghidini, Lucchini RS, for the test specimens supplied for this work and Arda Baytaroglu for the diligent support with sample preparation.

Appendix A. Supplementary data

Supplementary data to this article can be found online at https://doi.org/10.1016/j.jmrt.2024.07.107.

References

[1] Mädler K, Bannasch M. Materials used for wheels on rolling stock. Brandenburg-Kirchmöser, Germany 2006:7. URL, https://api.semanticscholar.org/CorpusID:53350908.
[2] Arnaiz Merino R. Development of railway wheels with alternative materials and production processes. Graz University of Technology; 2015.
[3] Bhadeshia HKDH. Cementite. Int Mater Rev 2020;65:1–27. https://doi.org/10.1080/09506608.2018.1560984.
[4] Atasoy OE, Özbilen S. Pearlite spheroidization. J Mater Sci 1989;24:281–7. https://doi.org/10.1007/BF00660968.
[5] Cvetkovski K, Ahlström J, Karlsson B. Thermal degradation of pearlitic steels: influence on mechanical properties including fatigue behaviour. Mater Sci Technol 2011;27:648–54. https://doi.org/10.1179/026708310X520538.
[6] Nikas D, Ahlström J. Characterization of microstructural changes in near pearlitic steels using orientation imaging microscopy - influence of predeformation on local sensitivity to thermal degradation. In: IOP Conf. Ser. Mater. Sci. Eng. Institute of Physics Publishing; 2015. https://doi.org/10.1088/1757-899X/89/1/012039. 89.
[7] Nikas D, Ahlström J, Malakizadi A. Mechanical properties and fatigue behaviour of railway wheel steels as influenced by mechanical and thermal loadings. Wear 2016;366–367:407–15. https://doi.org/10.1016/j.wear.2016.04.009.
[8] Faccoli M, Ghidini A, Mazzù A. Changes in the microstructure and mechanical properties of railway wheel steels as a result of the thermal load caused by shoe braking. Metall Mater Trans A Phys Metall Mater Sci 2019;50:1701–14. https://doi.org/10.1007/s11661-019-05135-x.
[9] Faccoli M, Ghidini A, Mazzù A. Experimental and numerical investigation of the thermal effects on railway wheels for shoe-braked high-speed train applications. Metall Mater Trans A Phys Metall Mater Sci 2018;49:4544–54. https://doi.org/10.1007/s11661-018-4749-2.
[10] Hu Y, Zhou L, Ding HH, Lewis R, Liu QY, Guo J, et al. Microstructure evolution of railway pearlitic wheel steels under rolling-sliding contact loading. Tribol Int 2021;154. https://doi.org/10.1016/j.triboint.2020.106685.
[11] Lu C, Mo J, Sun R, Wu Y, Fan Z. Investigation into multiaxial character of thermomechanical fatigue damage on high-speed railway brake disc. Vehicles 2021;3:287–99. https://doi.org/10.3390/vehicles3020018.
[12] Ribeiro Duarte AC, Mendes RS, Fontana M, Freitas da Silva FR, Pessoa de Castro GG, Cardoso Lins JF. Microstructural evolution of a pearlitic steel subjected to thermomechanical processing. Mater Res 2018;21. https://doi.org/10.1590/1980-5373-MR-2016-1065.
[13] Zhang MX, Pang JC, Qiu Y, Li SX, Wang M, Zhang ZF. Influence of microstructure on the thermo-mechanical fatigue behavior and life of vermicular graphite cast irons. Mater Sci Eng, A 2020;771. https://doi.org/10.1016/j.msea.2019.138617.
[14] Kihlberg E, Norman V, Skoglund P, Schmidt P, Moverare J. On the correlation between microstructural parameters and the thermo-mechanical fatigue performance of cast iron. Int J Fatig 2021;145:106112. https://doi.org/10.1016/j.ijfatigue.2020.106112.
[15] Malik IY, Lorenz U, Chugreev A, Behrens BA. Microstructure and wear behaviour of high alloyed hot-work tool steels 1.2343 and 1.2367 under thermo-mechanical loading. IOP Conf Ser Mater Sci Eng 2019;629. https://doi.org/10.1088/1757-899X/629/1/012011.
[16] Oudin A, Lamesle P, Penazzi L, Le Roux S, Rézaï-Aria F. Thermomechanical fatigue behaviour and life assessment of hot work tool steels. Eur Struct Integr Soc 2002;29:195–201. https://doi.org/10.1016/S1566-1369(02)80076-0.
[17] Teimourimanesh S, Vernersson T, Lundén R. Braking capacity of railway wheels — state-of-the-art survey. Thermal capacity of tread-braked railway wheels. 16th Int. Wheel. Congr 2010:18 pp.
[18] Caprioli S, Vernersson T, Handa K, Ikeuchi K. Thermal cracking of railway wheels: towards experimental validation. Tribol Int 2016;94:409–20. https://doi.org/10.1016/j.triboint.2015.09.042.
[19] Donzella G, Scepi M, Solazzi L, Trombini F. The effect of block braking on the residual stress state of a solid railway wheel. Proc Inst Mech Eng - Part F J Rail Rapid Transit 1998;212. https://doi.org/10.1243/0954409981530751.
[20] Rossmanith HP, Loibnegger F, Huber R. Thermomechanical fatigue fracture due to repeated braking of railway wheels. Mater Sci 2006;42:466–75.
[21] Landström EV, Steyn E, Vernersson T, Ahlström J. Thermomechanical testing and modelling of railway wheel steel. Int J Fatig 2023;168. https://doi.org/10.1016/j.ijfatigue.2022.107373.
[22] CEN. EN 13262: railway applications - wheelsets and bogies - wheels - product requirements. 2020. Brussels.
[23] Affeldt E, Loveday MS, Rinaldi Ricerca Sistema Energetico C. Validated code-of-practice for strain-controlled thermo-mechanical fatigue testing. 2006.
[24] Vernersson T. Temperatures at railway tread braking. Part 1: modelling. Proc Inst Mech Eng - Part F J Rail Rapid Transit 2007;221:167–82. https://doi.org/10.1243/0954409JRRT57.
[25] Vernersson T. Temperatures at railway tread braking. Part 2: calibration and numerical examples. Proc Inst Mech Eng - Part F J Rail Rapid Transit 2007;221:429–42. https://doi.org/10.1243/09544097JRRT90.
[26] Teimourimanesh S, Vernersson T, Lundén R. Modelling of temperatures during railway tread braking: influence of contact conditions and rail cooling effect. Proc Inst Mech Eng - Part F J Rail Rapid Transit 2014;228:93–109. https://doi.org/10.1177/0954409712465696.
[27] Ahlström J, Kabo E, Ekberg A. Temperature-dependent evolution of the cyclic yield stress of railway wheel steels. Wear 2016;366–367:378–82. https://doi.org/10.1016/j.wear.2016.04.002.
[28] Esmaeili A, Walia MS, Handa K, Ikeuchi K, Ekh M, Vernersson T, et al. A methodology to predict thermomechanical cracking of railway wheel treads: from experiments to numerical predictions. Int J Fatig 2017;105:71–85. https://doi.org/10.1016/j.ijfatigue.2017.08.003.
[29] Pavlina EJ, Van Tyne CJ. Correlation of Yield strength and Tensile strength with hardness for steels. J Mater Eng Perform 2008;17:888–93. https://doi.org/10.1007/s11665-008-9225-5.